Dynamics of the Acetyloxyl Radical Studied by Dissociative Photodetachment of the Acetate Anion†

Zhou Lu and Robert E. Continetti*

Department of Chemistry and Biochemistry, University of California, San Diego, 9500 Gilman Drive, La Jolla, California 92093-0340

Received: May 13, 2004; In Final Form: July 23, 2004

Photodetachment of the acetate anion, $CH_3CO_2^-$, and the subsequent dissociation dynamics of the $CH_3CO_2^\bullet$ radical were studied using photoelectron−photofragment coincidence spectroscopy at 355 and 257 nm. An upper limit to the adiabatic electron affinity (EA) of $CH_3CO_2^\bullet$, EA = 3.47 ± 0.01 eV was determined. Evidence for several low-lying electronic states of the $CH_3CO_2^\bullet$ radical were observed in the photoelectron spectra. Most $CH_3CO_2^\bullet$ radicals dissociated to $CH_3^\bullet + CO_2$ products with a large kinetic energy release ($\langle E_T \rangle / E_{avl} =$ 0.72 for 355-nm excitation) and an anisotropic angular distribution ($\beta \sim 1.2$), while ~10% of $CH_3CO_2^\bullet$ radicals were stable on the microsecond time scale at both wavelengths. Structured near-threshold photoelectron spectra at 355 nm were similar when photoelectrons were recorded in coincidence with either stable radicals or dissociation products, indicating a sequential dissociative photodetachment. Experiments were also carried out on $CD_3CO_2^-$ to aid in the interpretation of the photoelectron spectra and deduction of the dissociation mechanism.

Introduction

Oxygenated organic radicals are important in several complex environments. In the present work, the energetics and dynamics of the acetyloxyl radical formed by photodetachment of the acetate anion are studied. The acetyloxyl radical is a possible intermediate in the bimolecular collision of $CH_3O^\bullet + CO$,[1−3] an important process in atmospheric and combustion chemistry. In addition, carboxyl radicals $RCO_2^\bullet$ play significant roles in synthetic organic chemistry. Two well-known examples are the Kolbe and Hunsdiecker reactions,[4] both involving the unimolecular reaction step in which $RCO_2^\bullet$ radicals decompose into CO_2 and free radicals $R^\bullet$. Studies of the acetyloxyl radical, $CH_3CO_2^\bullet$, can thus provide insights into detailed reaction mechanisms in organic synthesis and the role this radical may play in oxidation and combustion phenomena.

The lifetime of $CH_3CO_2^\bullet$ and the reactivity of this radical or the decomposition product $CH_3^\bullet$ have been of interest to organic chemists for years.[5−13] Previous studies have focused on the kinetics and thermodynamics of decarboxylation. Most of these experiments made use of the dissociation of acetyl peroxide $(CH_3CO_2)_2$, which produces $CH_3CO_2^\bullet$ radicals followed by a subsequent dissociation to form $CH_3^\bullet$ and CO_2. The $CH_3^\bullet$ radicals can then react with other species in the reaction environment. By measuring the kinetics of these reactions, Herk et al. estimated the unimolecular decarboxylation rate constant of $CH_3CO_2^\bullet$ to be 10^9-10^{10} s^{-1} with an activation energy of 5 kcal/mol.[5] A similar study by Braun et al. with a more detailed kinetic treatment found a decomposition rate constant of 1.6×10^9 s^{-1} at 60 °C, and an activation energy $E_A = 6.6$ kcal/mol.[14] Taking into account the heat of combustion and the dissociation energy of $(CH_3CO_2)_2$, a heat of formation $\Delta_f H°_{298K} = -45 \pm 2$ kcal/mol and a decarboxylation exothermicity of 17 ± 5 kcal/mol were predicted for the acetyloxyl radical.[15]

Using the appearance energy method, mass-spectrometric measurements by Holmes et al. reported the heat of formation for $CH_3CO_2^\bullet$ to be $\Delta_f H°_{298K} = -51.7 \pm 3$ kcal/mol.[16] Experiments were also carried out to determine the electron affinity (EA) of $CH_3CO_2^\bullet$. These include Yamdagni and Kebarle's study of ion equilibria,[17] electron-impact ion appearance energy studies by Tsuda et al.[18] and Muftakhov et al.,[19] and electron attachment measurements by Wentworth and co-workers.[20] Wang and coworkers have also carried out a photodetachment study on the acetate anion, yielding an adiabatic EA ≈ 3.4 eV.[21] All these reported EA values show good agreement within a range from 3.2 to 3.4 eV.

Theoretical predictions of the structure and potential energy surfaces are difficult for the acetyloxyl radical because of the existence of several low-lying electronic states and symmetry breaking from C_{2v} to C_s symmetry.[2,3,22−27] The most recent studies include the ab initio calculations of Armstrong and coworkers on the acetyloxyl radical using MP2 and G2(MP2)/6-31G(D) methods[25,26] and a density functional theory (B3PW91/aug-cc-pVdz) calculation by Kieninger et al.[27] In these studies, two local minima were found, $^2A''(B_2)$ and $^2A'(A')$, along with two transition states $^2A'(B_2)$ and $^2A'(A_1)$. The symmetry terms are given for the overall $CH_3CO_2^\bullet$ radical (in C_s symmetry), and in parentheses, the symmetries of the molecular orbitals of the carboxyl group ($-CO_2^\bullet$) in either C_{2v} symmetry or C_s symmetry if the symmetry of that moiety is reduced by the pseudo-Jahn−Teller effect. The $^2A'(A')$ minimum and the $^2A'(B_2)$ transition state have one hydrogen atom lying in the plane of O−C−O (Figure 1a). The geometries of the $^2A''(B_2)$ minimum and the $^2A'(A_1)$ transition state, on the other hand, have one hydrogen located in the plane perpendicular to and bisecting the O−C−O plane (Figure 1b). The relative energies of these states vary considerably with the level of theory used, but the highest level ab initio results from Armstrong and coworkers indicate that the ground state is the $^2A''(B_2)$ state, with the $^2A'(A')$ state lying 0.1 eV higher at the G2(MP2) level of

† Part of the special issue "Tomas Baer Festschrift".

* Corresponding author. E-mail: rcontinetti@ucsd.edu.

10.1021/jp040355v CCC: $27.50
Published on Web 09/18/2004

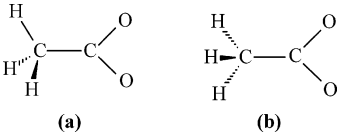

Figure 1. Structures of the CH_3CO_2 radical. (a) One hydrogen atom lies in the plane of O−C−O group. (b) One hydrogen atom is in the plane bisecting O−C−O group.

theory. The acetate anion is a closed-shell system, previously studied by Yu et al. at the MP2/6-31G(d) level,[26] with a $^2A'$-(A′) ground state, with an O−C−O bond angle of 130° compared to 121° for the analogous state in the radical. Armstrong and co-workers suggest that rotation about the C−C bond in the acetyloxyl radical may lead to $CH_3^\bullet + CO_2$ products with little or no barrier on the $^2A'(A_1)$ surface.

The formyloxyl radical $HCO_2^\bullet$ is the simplest analogue of $CH_3CO_2^\bullet$ and provides similar challenges for accurate calculations of its structure and energetics.[23,25−27] Unlike the lack of experimental results on $CH_3CO_2^\bullet$, however, photoelectron and photoelectron−photofragment coincidence (PPC) spectroscopy experiments on the formate anion HCO_2^- have provided insights into the electronic and vibrational structure of the $HCO_2^\bullet$ radical and the dissociation dynamics of $HCO_2^\bullet \rightarrow H + CO_2$.[28,29] To obtain spectroscopic and dynamics data on the $CH_3CO_2^\bullet$ radical, in the current work PPC spectroscopy was applied to study the dissociative photodetachment (DPD) of the acetate anion $CH_3CO_2^-$ and its deuterated form $CD_3CO_2^-$ in the gas phase. With different photon energies, the exploration of the low-lying electronic states of $CH_3CO_2^\bullet$ is possible, while experiments carried out near the photodetachment threshold yield high-resolution photoelectron spectra. Near-threshold measurements of the PPC spectra at 355 nm (3.49 eV) are reported along with an above-threshold measurement at 257 nm (4.82 eV). The branching between stable radicals and dissociation of the nascent $CH_3CO_2^\bullet$ radical is presented, along with a discussion of the mechanism and dissociation dynamics of $CH_3CO_2^\bullet$.

Experiment

The fast-ion-beam photoelectron−photofragment spectrometer used in this work has been previously described[30−32] and only the essential elements will be reviewed here. Room-temperature vapor of 20% acetic acid or deuterated acetic acid [prepared from CD_3CO_2D (99.5%, Cambridge Isotope Laboratory) and D_2O (99.9 atom %, Aldrich)] in aqueous solution was seeded in N_2O/Ar (∼13% N_2O, ∼87% Ar) and expanded through a 0.25-mm-diam nozzle pulsed at 1 kHz with a piezoelectric valve. A pulsed electric discharge was used to produce negative ions. The O^- produced by dissociative electron attachment to N_2O abstracted a proton from acetic acid, yielding the acetate anion. The fast ion beam of $CH_3CO_2^-$ ($m/e = 59$) or $CD_3CO_2^-$ ($m/e = 62$) at energies of 3 and 6 keV was mass-selected by time-of-flight (TOF) and perpendicularly intersected with linearly polarized laser pulses. Two different laser wavelengths were used: 355 nm (3.494 eV) generated by the third harmonic of an Nd:YAG laser (∼100 ps fwhm, Quantronix Model 116) and 257 nm (4.82 eV) from the third harmonic of a Ti:Sapphire laser (1.8 ps fwhm, Clark CPA 2000).

The full 4π sr solid angle of photoelectrons was collected by a space-focusing electron optics assembly first developed by Hayden and co-workers.[33] In the 257-nm experiments, the photoelectrons were extracted by a pulsed electric field of 8.9 V/cm toward the detector. In the near-threshold 355-nm experiments, a lower electric field of 1.0 V/cm was applied to achieve better resolution. The center of mass (CM) electron kinetic energies (eKE) and laboratory frame photoelectron angular distributions were calculated from the recorded time and position-of-arrival of the photoelectrons. The z velocity component of photoelectrons, perpendicular to the photoelectron detector face and derived from the photoelectron TOF, was the major factor limiting the resolution. To minimize this problem, a slice of the three-dimensional photoelectron distribution with small z velocity components in the CM is analyzed and the resulting photoelectron intensity distribution is corrected on the basis of the cylindrical symmetry about the electric vector of the laser.[34] This required the photoelectron data to be recorded with the laser electric vector along the direction of the ion beam, parallel to the face of the photoelectron detector. The resulting energy resolution is $\Delta E/E \approx 12\%$ (fwhm) as determined by the photodetachment of I^- at 257 nm. To reduce laser-generated photoelectron background in the 257-nm experiments, only those electrons coincident with at least one photofragment or the stable neutral product were collected.

Undetached anions were deflected out of the beam into a microchannel-plate-based ion detector. The stable free radicals and neutral photofragments formed by photodetachment were detected by a 4-cm-diam two-particle time- and position-sensitive detector, with a 7-mm-diam beam block at the center.[30] By adjusting the vertical position of the neutral particle detector, the ion beam can be either centered on the beam block or off-centered on one of the two detector halves. In the centered case, only photofragments with sufficient recoil velocities to clear the beam block are detected. In the off-centered case, photofragments recoiling along the ion beam and nondissociative stable radicals are detectable. Conservation of linear momentum between the coincident photofragments determines the product mass ratio and the CM kinetic energy release, E_T, for the dissociation event. The detector acceptance function (DAF) for detecting coincident photofragments with the neutral particle detector is a function of the kinetic energy of the ion beam, the mass ratios of the dissociation products, the translational energy release during the dissociation, and the position of the detector. Numeric correction for the DAF has been previously derived and is used here to convert the measured $N(E_T)$ distributions into product translational energy $P(E_T)$ distributions.[35] The dissociative photodetachment $O_4^- + h\nu \rightarrow O_2 + O_2 + e^-$ at 257 nm was used for calibration, yielding a resolution of $\Delta E_T/E_T \approx 10\%$.

Results

Photoelectron Spectra. The photoelectron kinetic energy spectrum of acetate anion recorded at 3.494 eV (355 nm) is shown in Figure 2a. As discussed in the Experimental Section, this spectrum represents the probability of photoelectrons P(eKE) integrated over the full 4π sr. A narrow distribution near eKE = 0.0 eV is observed, indicating that this photon energy is close to the photodetachment threshold. Two peaks are observed in the spectrum, one at 0.003 eV, and the other at 0.026 eV (peak I in Figure 2a). To reveal the origin of the 0.023 eV (185 cm^{-1}) energy spacing, the P(eKE) spectrum of the deuterated acetate anion, $CD_3CO_2^-$ (Figure 2b), was collected under the same experimental conditions. The two spectra have nearly identical features, indicating that the observed structure is not related to C−H vibrational modes and that zero-point energy differences between the anion and neutral radical nearly cancel. Assuming that the peak at 0.026 eV is the electronic origin, an upper limit to the adiabatic electron affinity (AEA) is 3.47 ± 0.01 eV, in good agreement with the lower resolution experiments of Wang and co-workers.[21] The precision of ±0.01

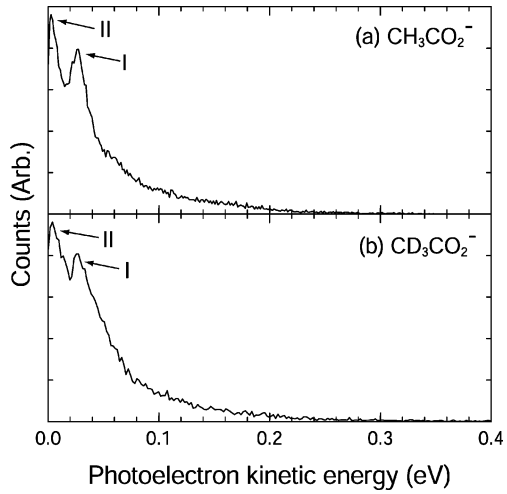

Figure 2. Near-threshold photoelectron spectra of (a) $CH_3CO_2^-$ and (b) $CD_3CO_2^-$ at 355 nm (3.49 eV). The position of peak I is used to calculate the upper limit of adiabatic EA of $CH_3CO_2^{\bullet}$ and $CD_3CO_2^{\bullet}$.

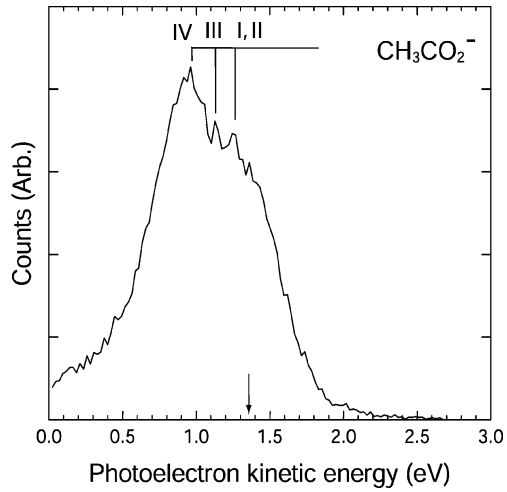

Figure 3. Photoelectron spectrum of $CH_3CO_2^-$ at 257 nm (4.82 eV). The arrow points to EA determined from Figure 2.

eV in this case refers to the measurement itself—the assignment will be discussed further in Sections 4.1 and 4.2 below. The photoelectron images recorded at 355 nm are not shown here but are consistent with *s*-wave photodetachment with a nearly isotropic angular distribution near threshold.

A high-energy tail extending above 0.2 eV is seen in both of the P(eKE) spectra in Figure 2, however, which is likely to arise from photodetachment of vibrationally excited anions. The acetate anions in this experiment were generated in a pulsed discharge, with vibrational temperatures expected to be 300 K or greater. A RB3LYP/aug-cc-pVDZ calculation of the vibrational frequencies in the anion was carried out. Using the calculated vibrational frequencies, the vibrational partition function was evaluated indicating that a tail of this magnitude can arise from a vibrational temperature of ≈400 K, ignoring any Franck−Condon effects, consideration of which are beyond the scope of the present work given the complexity of the electronic structure of the acetyloxyl radical. The observed high-energy tail suggests that the upper bound for the EA = 3.47 ± 0.01 eV can be no more than 0.2 eV too high.

The P(eKE) spectrum of $CH_3CO_2^-$ obtained at a photon energy of 4.82 eV (257 nm) is shown in Figure 3. Since the photon energy of 4.82 eV is no longer near threshold, the eKE resolution is worse and the fine structure observed in the 3.49 eV spectra in Figure 2 is not seen here. However, two new

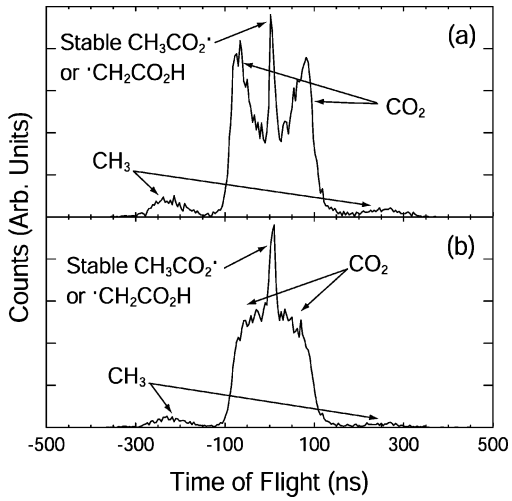

Figure 4. Time-of-flight (TOF) spectra of neutral products in photodetachment of $CH_3CO_2^-$ at 355 nm (3.49 eV). (a) Electric vector of laser parallel to the direction of ion beam (perpendicular to the face of neutral particle detector); (b) electric vector of laser perpendicular to the direction of ion beam (parallel to the face of neutral particle detector). The abscissa here is the relative TOF with zero as the TOF of undissociated $CH_3CO_2^{\bullet}$ (or $^{\bullet}CH_2CO_2H$).

poorly resolved features are observed when compared with the spectrum at 3.49 eV: 1.14 eV (peak III in Figure 3) and 0.94 eV (peak IV), while the third feature at 1.30 eV is consistent with the near-threshold photodetachment observed at $E_{h\nu} = 3.49$ eV. Comparison of Figures 2 and 3 shows the eKE spectrum taken at 257 nm is significantly broadened because of the loss of resolution at high eKE. The assignment of the features (III) and (IV) must be taken as tentative given the signal-to-noise of the measurement. The photoelectron images recorded at 257 nm are not reported here, but indicate that the photoelectron angular distribution peaks perpendicular to the laser electric vector at this wavelength.

Photofragment Spectra. The time-of-flight (TOF) spectra of the resultant neutral particles after photodetachment of the acetate anion at $E_{h\nu} = 3.49$ eV are shown in Figure 4. The ion beam was set off-center on the neutral particle detector for this measurement. The photofragment TOF spectra at $E_{h\nu} = 4.82$ eV are not presented here because they are very similar to the spectra in Figure 4. The abscissa is the time of arrival of the neutral particles relative to the TOF of the center-of-mass at zero. Negative TOF corresponds to particles recoiling forward in the direction of the ion beam velocity and positive TOF corresponds to particles recoiling backward. These fast-ion-beam TOF spectra are analogous to the Doppler spectra frequently measured in optical studies of reaction dynamics.[36,37] The sharp peak at 0 ns in the TOF spectra in Figure 4 results from a stable neutral radical with the empirical formula $C_2H_3O_2$. The broad feature around the $C_2H_3O_2$ peak result from CO_2 molecules produced in the dissociation of the $CH_3CO_2^{\bullet}$, while the smaller wings at larger positive and negative TOF are from lighter $CH_3^{\bullet}$ radical products scattered forward and backward along the beam. In Figure 4, the CO_2 peaks are significantly higher than $CH_3^{\bullet}$ peaks and an asymmetry in peak heights is also seen when comparing the peaks at negative TOF with those at positive TOF. This is a result of the finite DAF for detection of the dissociation products of $CH_3CO_2^{\bullet}$ at this beam energy. The relatively large E_T and the mass of $CO_2/CH_3^{\bullet} = 44/15$ results in most of the $CH_3^{\bullet}$ products recoiling out of the beam and missing the neutral particle detector. Similarly, the particles at negative TOF have larger laboratory velocities and recoil less out of the beam before reaching the detector and are thus

detected with higher efficiency. The branching ratio between stable $C_2H_3O_2$ radical and dissociation products is ≈1:9 based on measuring the relative intensities of the CO_2 and stable radical peaks in Figure 4 under the assumption that the detection efficiencies are equal for both particles that strike the detector. TOF spectra of $C_2D_3O_2$ radicals gave similar results, indicating that the branching between stable radicals and dissociation products is not sensitive to isotopic substitution of deuterium for hydrogen.

Comparison of Figure 4a and 4b shows that the dissociation products are more separated in TOF when the laser vector is along the ion beam. This anisotropic photofragment angular distribution implies that rupture of the carbon−carbon bond occurs promptly on the time scale of molecular rotation. As discussed by Zare and others,[38] the photofragment angular distribution in the electric-dipole approximation is given by

$$I(E_T,\theta) = \frac{\partial\sigma(E_T)}{\partial\Omega} = \frac{\sigma_{tot}}{4\pi}[1 + \beta(E_T)\cdot P_2(\cos\theta)] \qquad (1)$$

where σ_{tot} is the total photodissociation cross section, θ is the polar angle between the photofragment recoil and the laser electric vector, $P_2(\cos\theta)$ is the second-order Legendre polynomial in $\cos\theta$, and $\beta(E_T)$ is an energy-dependent anisotropy parameter, ranging between −1 and 2. Fitting the photofragment angular distributions and the time-of-flight spectra following correction for the DAF[35] shows an energy-averaged anisotropy parameter $\beta \approx 1.2 \pm 0.2$, corresponding to a predominantly $\cos^2\theta$ distribution. This shows that DPD of the acetate anion yields an anisotropic photofragment angular distribution, similar to the direct DPD of O_4^- previously studied in this laboratory.[39]

The DAF-corrected translational energy release distributions, $P(E_T)$, for the DPD of $CH_3CO_2^-$ and $CD_3CO_2^-$ at both $E_{h\nu}$ = 3.49 and 4.82 eV are plotted in Figure 5. At $E_{h\nu}$ = 3.49 eV, $P(E_T)$ for $CH_3CO_2^-$ peaks at 0.65 eV (Figure 5a, dashed line), with a relatively narrow distribution. In DPD at $E_{h\nu}$ = 4.82 eV, the $P(E_T)$ (solid line in Figure 5a) is nearly the same on the low-energy side as the 3.49 eV distribution; however, at high E_T in the 4.82 eV distribution, $P(E_T)$ is broader, and the peak shifts to 0.80 eV. The translational energy distribution for the DPD of $CD_3CO_2^-$ shown in Figure 5b is similar, with the distribution shifted to lower E_T at both wavelengths compared with the $CH_3CO_2^-$ data: $P(E_T)$ peaks at 0.60 eV at $E_{h\nu}$ = 3.49 and 0.69 eV at $E_{h\nu}$ = 4.82 eV, respectively.

Photoelectron−Photofragment Correlation Spectra. The unique feature of our apparatus is that it allows the coincident measurement of the photoelectron and photofragments, revealing the partitioning of the available kinetic energy among the products. One interesting observation is that the P(eKE) spectra measured in coincidence either with only the stable $C_2H_3O_2$ radical or with only the $CH_3^\bullet + CO_2$ products are indistinguishable within the signal-to-noise ratio of the measurement. This phenomenon will be discussed in detail in section 4.1 below. Figure 6 shows the photoelectron−photofragment kinetic energy correlation spectra, N(eKE, E_T), as two-dimensional gray scale histograms in which the intensity of each point represents the number of events with specific eKE and E_T values in the DPD of $CH_3CO_2^-$. On the left and the bottom of each correlation spectrum are the raw N(eKE) and $N(E_T)$ spectra, respectively. These spectra are uncorrected for any DAF effects and are obtained by integrating over the complementary variables in the two-dimensional correlation spectrum. The N(eKE) spectrum for $E_{h\nu}$ = 4.82 eV seen in Figure 6b exhibits a different intensity distribution than the higher-resolution sliced and DAF-corrected P(eKE) spectrum shown in Figure 3. This occurs because it is not possible to carry out the DAF-correction for the photoelectrons in the correlated data, so the resolution is reduced and the intensity distribution is altered. The experimental value for the maximum kinetic energy release (KE_{MAX}) for all products in the DPD reaction ($CH_3CO_2^- + h\nu \rightarrow CH_3^\bullet + CO_2 + e^-$) is typically determined from the contour at 5% of the peak, representing the level of false coincidences expected in the experiment.[30] The value of $KE_{MAX} = 0.93 \pm 0.05$ eV obtained from the higher-resolution near-threshold photodetachment data at $E_{h\nu}$ = 3.49 eV is shown by the diagonal line in Figure 6a. In Figure 6b, the $E_{h\nu}$ = 4.82 eV data is shown, along with $KE_{MAX} = 2.26 \pm 0.05$ eV, as derived from the data in Figure 6a and the photon energy difference. As Figure 6b shows, this value of KE_{MAX} cuts through a significant fraction of the data, as a result of the much lower N(eKE) resolution this far above threshold. The KE_{MAX} value of 0.93 eV obtained from the near-threshold photodetachment at $E_{h\nu}$ = 3.49 eV is the most reliable and shows that 2.56 eV is required to dissociate $CH_3CO_2^- \rightarrow CH_3^\bullet + CO_2 + e^-$.

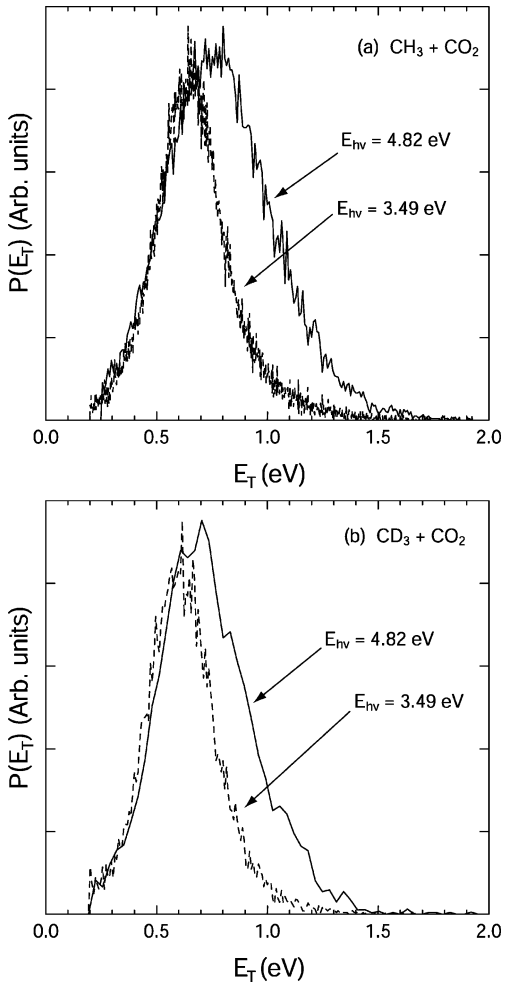

Figure 5. Translational energy release spectra, $P(E_T)$, of the photofragments in the dissociative photodetachment of (a) $CH_3CO_2^-$, (b) $CD_3CO_2^-$. The solid lines in both a and b represent the $N(E_T)$ recorded at 257 nm (4.82 eV). The dashed lines represent $N(E_T)$ at 355 nm (3.49 eV).

At a photon energy of 3.49 eV, all events in the correlation spectrum are compressed at the bottom owing to the small distribution of eKE. In the correlation spectrum when $E_{h\nu}$ = 4.82 eV, there are two regions corresponding to the two broad features in the N(eKE) spectrum with slightly different translational energy release, E_T (Figure 6b). The region with larger eKE corresponds to the peak at 1.30 eV in the N(eKE) spectrum

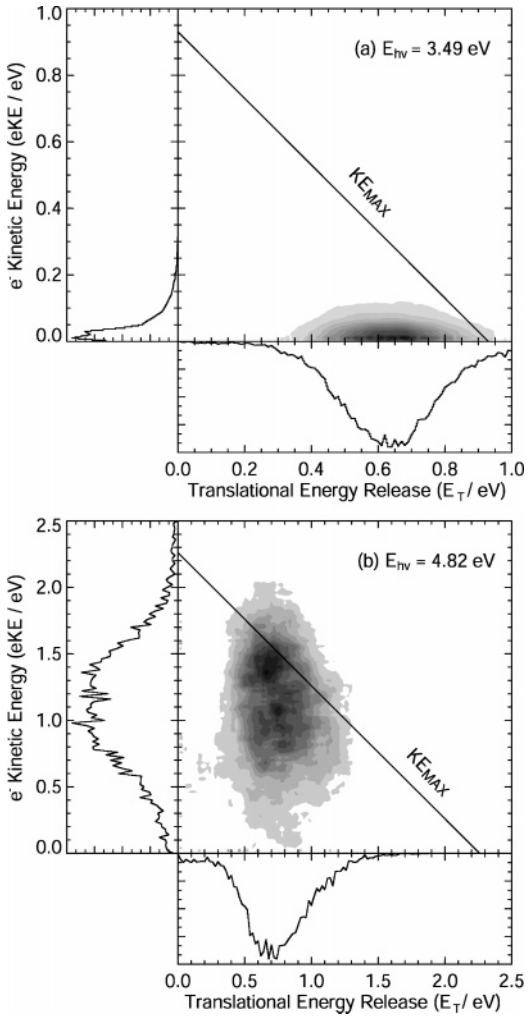

Figure 6. Photoelectron−photofragment translational energy correlation spectra, N(E_T, eKE), of $CH_3CO_2^-$ at (a) 355 nm (3.49 eV), (b) 257 nm (4.82 eV). The photoelectron N(eKE) spectra are shown along the *y*-axis and the photofragment N(E_T) spectra are shown along the *x*-axis. The diagonal lines represent KE_{MAX} at E_{hv} = 3.49 eV as described in the text.

recorded at the same photon energy. The other region corresponds to the features at eKE = 0.94 and 1.14 eV. These lower eKE features arise from new electronic states accessed at E_{hv} = 4.82 eV and lead to the larger E_T release seen in the high-energy tail on the P(E_T) spectra at this photon energy in Figure 5. The total kinetic energy, KE_{total} = eKE + E_T, is smaller for the lower eKE features, implying that the $CH_3^\bullet + CO_2$ formed by dissociation of these new electronic states are more vibrationally or rotationally excited since there are no low-lying electronic states of the products.

Discussion

The spectra presented here provide insights into the energetics and dynamics of the $CH_3CO_2^\bullet$ radical formed in the photodetachment of $CH_3CO_2^-$. In section 4.1, possible mechanisms are suggested on the basis of the PPC spectra and TOF of the neutral products. The energetics of the nascent $CH_3CO_2^\bullet$ radical from the P(eKE) spectra and comparison with theoretical predictions are discussed in section 4.2. In section 4.3, an impulsive model is applied to interpret the energy partitioning among the dissociation products. Finally, the possibility of ionic photodissociation channels competing with DPD is considered.

Reaction Mechanism. The TOF spectra of the neutral particles in Figure 4 reveal two channels after the photodetachment of the $CH_3CO_2^-$: dissociation into $CH_3^\bullet + CO_2$ and a minor channel yielding the stable radical $C_2H_3O_2^\bullet$. The two most likely structures of $C_2H_3O_2^\bullet$ radical are the acetyloxyl radical, $CH_3CO_2^\bullet$, and the carboxyl-methyl radical isomer $^\bullet CH_2CO_2H$. The present experiments cannot distinguish between these two isomers but provide the first direct evidence that stable radicals can be produced by photodetachment of the acetate anion in the gas phase. This result contradicts previous suggestions that all the $CH_3CO_2^\bullet$ radicals dissociate on ns time scales.[5] Thus, in some combustion and organic synthesis processes, not only $CH_3^\bullet$ but also the nondissociative $CH_3CO_2^\bullet$ or $^\bullet CH_2CO_2H$ radicals may play roles in the reaction mechanisms and kinetics. It is also possible that in condensed phase environments, the nascent $CH_3CO_2^\bullet/^\bullet CH_2CO_2H$ radical is stabilized. In the experiments at a beam energy of 3 keV, it takes approximately 10 μs for $C_2H_3O_2$ to travel from the interaction region to the neutral particle detector, providing a lower limit for the lifetime of the stable $C_2H_3O_2$ radical of $\sim$10 μs under collision-free conditions.

As mentioned in section 3.3 above, the P(eKE) spectra measured in coincidence either with only stable $C_2H_3O_2$ radicals or with only the $CH_3^\bullet + CO_2$ products are indistinguishable within the signal-to-noise of the measurement. This implies that instead of a transition directly from the acetate anion to a repulsive potential surface of the neutral radical, the removal of one electron from $CH_3CO_2^-$ places the $CH_3CO_2^\bullet$ radical into some intermediate states. Following the production of the nascent $CH_3CO_2^\bullet$, the system rapidly (faster than molecular rotation) evolves to either produce the stable $CH_3CO_2^\bullet/^\bullet CH_2CO_2H$ radical or the dissociation products. Given the small branching ratio to stable radicals, we cannot unambiguously say at this time whether there is some internal energy dependence in the product branching process, but there is no gross dependence. If the observed stable radical is $CH_3CO_2^\bullet$, the intermediate species may be one of the transition states or low-lying excited states theoretically predicted for this species, as reviewed in the Introduction:

$$CH_3CO_2^- + h\nu \rightarrow CH_3CO_2^{\cdot *} + e^- \rightarrow CO_2 + CH_3^\cdot + e^- \quad (90\%)$$

$$\downarrow$$

$$CH_3CO_2^\cdot + e^- \quad (10\%)$$

Formation of the isomeric stable radical $^\bullet CH_2CO_2H$ from the nascent $CH_3CO_2^\bullet$ is also possible. Although the barrier of an intramolecular hydrogen atom transfer forming $^\bullet CH_2CO_2H$ radical from $CH_3CO_2^\bullet$ is still unknown, this process is energetically favorable,[27,40] with an energy difference of $\sim$0.8 eV between the lowest state of $CH_3CO_2^\bullet$ observed in this work and $^\bullet CH_2CO_2H$ reported in ref 40 (See Table 1 and Figure 7). Direct production of the $^\bullet CH_2CO_2H$ radical from photodetachment of the isomeric anion $CH_2CO_2H^-$ is unlikely on energetic grounds since the EA $\approx$ 1.9 eV for the $^\bullet CH_2CO_2H$ radical[19] is inconsistent with the P(eKE) spectra presented. Thus, the $^\bullet CH_2CO_2H$ radical can only originate from the isomerization process: $CH_3CO_2^\bullet \rightarrow {}^\bullet CH_2CO_2H$. The observation that the branching ratio between stable radicals and dissociation products is not sensitive to deuteration indicates that if isomerization occurs, it must happen after formation of a metastable state of the $CH_3CO_2^\bullet/CD_3CO_2^\bullet$ radical as opposed to directly competing with the prompt dissociation channel.

This model, photodetachment to an intermediate state, followed by a rapid evolution to either one or more stable products and a dissociative final state can explain the apparently conflicting phenomena observed—the existence of the stable $C_2H_3O_2$ radical with a lifetime longer than 10 μs and the anisotropic photofragment angular distribution indicative of a

TABLE 1: Energetics Data[a]

	relative energy (eV)	ref
$CH_3CO_2^-$	0.00 ± 0.14	b
$CH_3CO_2^\bullet$ (I) + e^-	3.47 ± 0.01	
$CH_3CO_2^\bullet$ (II) + e^-	3.49 ± 0.01	
$CH_3CO_2^\bullet$ (III) + e^-	3.68 ± 0.1	
$CH_3CO_2^\bullet$ (IV) + e^-	3.88 ± 0.1	
$CH_3^\bullet + CO_2 + e^-$	2.56 ± 0.05	
	2.67 ± 0.14	b
$^-CH_2CO_2H$	0.86 ± 0.2	c
$^\bullet CH_2CO_2H + e^-$	2.64 ± 0.2	d
$CH_3^\bullet + CO_2^-$	3.16 ± 0.2	e
$CH_3^- + CO_2$	2.48 ± 0.06	f

[a] All values listed are relative energies using the ground state of $CH_3CO_2^-$ as reference level. [b] Reference 42. [c] Reference 53. [d] Reference 40. [e] This value is determined by the energy level of $CH_3^\bullet + CO_2 + e^-$ measured in this work and the EA of CO_2 from ref 49. [f] This value is determined by the energy level of $CH_3^\bullet + CO_2 + e^-$ measured in this work and the EA of CH_3 from ref 51.

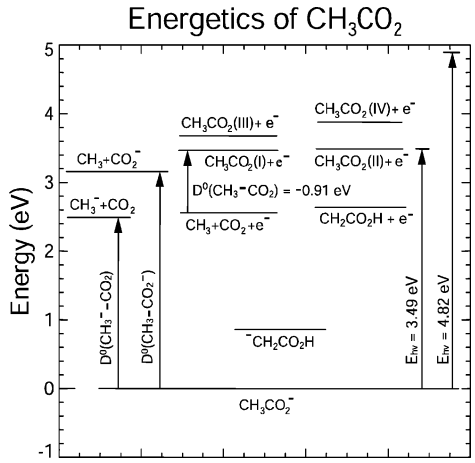

Figure 7. Energetics of the dissociative photodetachment of $CH_3CO_2^-$ in eV, relative to the ground state of $CH_3CO_2^-$. The energy of the $CH_3 + CO_2^-$ channel is determined by the EA of CO_2,[49] and the energy of $CH_3^- + CO_2$ is determined from the EA of CH_3 [51] and the energetics for the DPD yielding $CH_3^\bullet + CO_2 + e^-$ measured in this work. The energy of $^\bullet CH_2CO_2H$ is obtained from ref 40 and energy of $^-CH_2CO_2H$ from ref 53.

prompt decarboxylation process occurring in much less than a molecular rotational period. Although the preponderance of the radicals end up on the dissociative surface, some of them find at least a metastable state and possibly undergo an isomerization to the more stable carboxyl-methyl radical, $^\bullet CH_2CO_2H$. This model needs the verification of reliable calculations that are beyond the scope of the present study.

Energetics and Dissociation Mechanism of the $CH_3CO_2^\bullet$ Radical. Threshold photodetachment at $E_{h\nu} = 3.49$ eV provides a high-resolution P(eKE) spectrum which is helpful to resolve the low-lying excited states of $CH_3CO_2^\bullet$. As mentioned in Section 3.1, the P(eKE) spectra are nearly identical for $CH_3CO_2^-$ and $CD_3CO_2^-$, indicating the fine structure obtained at $E_{h\nu} = 3.49$ eV does not originate from C−H vibrations. Moreover, the energy spacing of 0.023 eV ($\sim$185 cm^{-1}) is close to none of the vibrational frequencies of the $CH_3CO_2^\bullet$ calculated by Rauk et al.[25] and known vibrational energy levels of acetic acid, CH_3CO_2H.[41] As discussed in the Introduction, there is a significant change in O−C−O bending angle expected on photodetachment, however, the O−C−O bend in the acetyloxyl radical is predicted to be about 600 cm^{-1} by comparison with the acetate anion and formyloxyl radical.[28] A likely explanation for these resolved features is that two nearly degenerate electronic states are produced. This is supported by Neumark and co-workers' photodetachment study on the formate anion, HCO_2^-,[28] in which they reported the energy spacing between the ground and first electronic states to be 0.027 eV. It is also possible that some of the original acetate anions are vibrationally excited so the observed energy spacing could be the combination of the vibrational frequencies in the $CH_3CO_2^-$ and neutral CH_3-$CO_2^\bullet$ radicals. Although we cannot completely rule out this possibility, it is not likely because the fine structure was found unchanged even when different ion source conditions were employed. These two energy states, together with the two higher-lying states tentatively inferred from the P(eKE) spectrum at the photon energy of 4.82 eV, are shown in the Table 1 and in the energy diagram in Figure 7. The observed electron affinity of $CH_3CO_2^\bullet$ is larger than the older values calculated from the previously reported heat of formation data of $CH_3CO_2^\bullet$ discussed in the Introduction[15,16] but is consistent with the lower resolution photoelectron spectroscopy measurements of Wang and co-workers.[21]

As discussed in the Introduction, the electronic structure of the $CH_3CO_2^\bullet$ radical is complex owing to the presence of the O−C−O moiety and is analogous to the well-studied $HCO_2^\bullet$ radical. As discussed by Rauk et al.,[25] the lowest energy minimum for the $CH_3CO_2^\bullet$ radical is $^2A''(B_2)$ (Figure 1b), while a transition state, $^2A'(B_2)$ (Figure 1a), separates the two symmetric $^2A''(B_2)$ geometries when the CH_3 group rotates about the C−C bond. Another minimum $^2A'(A')$ (Figure 1a, but with the O−C−O moiety distorted from C_{2v} symmetry) is separated from the dissociation products $CH_3^\bullet + CO_2$ by the transition state $^2A'(A_1)$ (Figure 1b). At the G2(MP2)/6-31G(D) level, Rauk et al. found the $^2A''(B_2)$ and $^2A'(A')$ minima to be separated by 0.1 eV, nearly degenerate as are the two resolved peaks in the P(eKE) spectra. These are presumably the two states we are observing, however, an unambiguous assignment of the ground state is not possible at this time.

The previous geometry optimization of the acetate anion by Yu et al. using MP2/6-31G(D) shows the minimum for $CH_3CO_2^-$ is similar to the $^2A'(A')$ minimum of the $CH_3CO_2^\bullet$ radical in Figure 1a.[26] A DFT calculation (RB3LYP/aug-cc-pvdz) we carried out, on the other hand, indicates that the $CH_3CO_2^-$ minimum has a geometry similar to Figure 1b, with one H−C−C bond perpendicular to the O−C−O bond. These conflicting results are consistent with the observation that the torsional motion of the $CH_3^\bullet$ group in the $CH_3CO_2^-$ anion had nearly no barrier in our DFT calculations. Thus, it is possible that anion photodetachment projects onto both of the low-lying states of the $CH_3CO_2^\bullet$ radical in accordance with the Franck−Condon principle. Armstrong and co-workers suggest that rotation of the methyl radical about the C−C bond can lead to rapid dissociation to $CH_3^\bullet + CO_2$ via the $^2A'(A_1)$ transition state. Potential energy surfaces derived from high-level multireference configuration interaction calculations would be helpful for a Franck−Condon simulation of the P(eKE) spectra and further examination of the dissociation mechanism.

Dissociation Dynamics. The KE_{MAX} value shown on the photoelectron−photofragment correlation spectra defines the maximum available energy partitioned into the translational degrees of freedom of the photoelectron and two photofragments in a DPD event, which can be calculated by

$$KE_{MAX} = h\nu - \Delta H_{f,0K}^\circ(CH_3^\bullet) - \Delta H_{f,0K}^\circ(CO_2) + \Delta H_{f,0K}^\circ(CH_3CO_2^-) \quad (2)$$

In eq 2, $\Delta H_{f,0K}^\circ$ is the standard enthalpy of formation at 0 K of the designated species in gas phase. Assuming that the KE_{MAX}

value measured in the threshold photodetachment experiment corresponds to some $CH_3^\bullet + CO_2 + e^-$ products in their ground vibrational and electronic states, this dissociation asymptote is 2.56 ± 0.05 eV above $CH_3CO_2^-$ as shown in Figure 7. This value is 0.11 eV smaller than the results calculated on the basis of the thermodynamics data from the NIST Standard Reference Database.[42] Combining the present results with the EA of 3.47 eV, the dissociation energy of the $CH_3CO_2^\bullet$ radical into $CH_3^\bullet + CO_2$ is $D_0(CH_3 - CO_2) = -0.91 \pm 0.05$ eV. These results are summarized in Table 1 and Figure 7.

Unlike the DPD study on HCO_2^-,[29] no vibrational progressions were observed in the P(E_T) distributions for the DPD of $CH_3CO_2^-$ and $CD_3CO_2^-$ because both CO_2 and $CH_3^\bullet$ (or $CD_3^\bullet$) can be vibrationally and rotationally excited. The average internal energy ($\langle E_{int} \rangle$) partitioned into the dissociation products is $\langle E_{int} \rangle = 0.26$ eV (2100 cm^{-1}) for $CO_2 + CH_3^\bullet$ and $\langle E_{int} \rangle = 0.31$ eV (2500 cm^{-1}) for $CO_2 + CD_3^\bullet$ at 355 nm, calculated from KE_{MAX}, the average translational energy release $\langle E_T \rangle$, and the near-threshold eKE. When the C−C bond breaks in the CH_3-$CO_2^\bullet$ radical, the most significant geometric changes are the change of the CH_3 group from a pyramidal to a planar shape and the relaxation of the bent O−C−O moiety to linear CO_2.[43] The major vibrational excitations expected in the products are thus the out-of-plane umbrella mode of $CH_3^\bullet$ and the degenerate bending mode of CO_2. The umbrella (ν_2) frequency is 608.3 cm^{-1} for $CH_3^\bullet$ radical[44] and 457.8 cm^{-1} for $CD_3^\bullet$,[45] while the bending frequency of CO_2 is $\nu_2 = 667.3$ cm^{-1}.[46] Therefore, in the $CH_3^\bullet + CO_2$ system, the most probable vibrational excitation is characterized by the sum of vibrational quantum numbers, $v_2(CH_3^\bullet) + v_2(CO_2) = 3$ or 4. In the $CD_3^\bullet + CO_2$ system, $CD_3^\bullet$ is expected to exhibit higher vibrational excitation v_2 owing to the smaller vibrational quanta.

The observed energy partitioning in the DPD of $CH_3CO_2^-$ can be compared to the pure impulsive model used by Busch and Wilson and later extended by Houston and co-workers.[47,48] Using the pure impulsive model, all the chemical bonds are assumed to be soft except for the one that breaks in the dissociation. In other words, all the atoms not involved in the breaking bond stay still as "spectators". Given a dissociation AB → A + B by breaking a chemical bond α-β, with atom α in A and atom β in B, the CM translational energy release E_T is given by

$$E_T = \frac{\mu_{\alpha\beta}}{\mu_{AB}} E_{avl} \tag{3}$$

where E_{avl} is the available energy, μ_{AB} is the reduced mass of A and B, and $\mu_{\alpha\beta}$ is the reduced mass of α and β. The translational and internal energy partitioned into the fragment A can be calculated separately by

$$E_T(A) = \frac{\mu_\alpha \beta}{m_A} E_{avl} \tag{4}$$

$$E_{int}(A) = \left(\frac{1}{m_\alpha} - \frac{1}{m_A}\right) \mu_{\alpha\beta} E_{avl} \tag{5}$$

with analogous equations for fragment B, where m_A, m_B, m_α, and m_β are the masses for A, B, α, and β, respectively. The pure impulsive model can also be used to predict product rotational excitation when the α−β bond is not directed to the CM of A or B; however, in the present experiments product rotational and vibrational excitation cannot be resolved, so only the total internal energy will be considered.

TABLE 2: Energy Partitioning in the DPD of $CH_3CO_2^-$ and $CD_3CO_2^-$ at $E_{h\nu} = 3.49$ eV

		pure impulsive model		experimental values (355 nm)	
		f_T	f_{int}	f_T	f_{int}
$CO_2 + CH_3^\bullet$	CO_2	0.14	0.36		
	$CH_3^\bullet$	0.40	0.10		
	sum	0.54	0.46	0.72	0.28
$CO_2 + CD_3^\bullet$	CO_2	0.14	0.36		
	$CD_3^\bullet$	0.33	0.17		
	sum	0.47	0.53	0.67	0.33

Using eqs 3−5, the energy partitioning predicted by the impulse model at 355 nm can be calculated. Here, the value of KE_{MAX} is used as E_{avl} since eKE is nearly zero at this wavelength. The results of this calculation are listed in Table 2, where $f_T = E_T/E_{avl}$, and $f_{int} = E_{int}/E_{avl}$, with comparisons to the experimental values $f_T = \langle E_T \rangle/E_{avl}$ and $f_{int} = \langle E_{int} \rangle/E_{avl}$. The results in Table 2 illustrate that in addition to the higher density of internal energy states in the $CD_3^\bullet$ product, the isotopic shift in the impulsive partitioning of momentum also causes the shift of the P(E_T) peak to a lower value for $CD_3CO_2^-$ in Figure 5. The pure impulsive model is seen to overestimate the internal energy compared with the experimental results, indicating that the spectator bonds are not entirely "soft". This is not surprising for the relatively high-frequency C−H and C−D vibrations. This model also does not account for vibrational excitation in the nascent $CH_3CO_2^\bullet$ induced by Franck−Condon photodetachment.

Competition between Photodetachment and Ionic Photodissociation. Up to this point, only the DPD mechanism has been discussed. However, it is also important to consider another possible reaction path: photodissociation into one neutral and one anion, followed by either autodetachment or photodetachment of the secondary anion by a second photon.

The reaction: $CH_3CO_2^- + h\nu \rightarrow CO_2^- + CH_3^\bullet \rightarrow CO_2 + CH_3^\bullet + e^-$ is not energetically possible because CO_2^- is ≈0.60 eV higher than CO_2 in the energy diagram.[49,50] As shown in Figure 7, $E_T = E_{h\nu} - D°(CH_3{-}CO_2^-)$. At $E_{h\nu} = 3.49$ eV, this would require E_T to be smaller than 0.33 eV, which conflicts with the fact that in Figure 5a, P(E_T) begins to rise rapidly above 0.30 eV.

The other reaction path $CH_3CO_2^- + h\nu \rightarrow CH_3^- + CO_2 \rightarrow CH_3^\bullet + CO_2 + e^-$ needs more careful inspection. The methyl radical, $CH_3^\bullet$ has a small EA = 0.08 ± 0.03 eV measured by Ellison et al.[51] Wenthold and Squires studied the collision-induced dissociation (CID) of $CH_3CO_2^-$ and reported the dissociation energy, $D°[CH_3^-{-}CO_2]$, of 2.50 ± 0.11 eV.[40] The energetics reported in Figure 7 show the result for the upper limit to the bond dissociation energy $D_0[CH_3^-{-}CO_2]$ found in the present experiment is 2.48 ± 0.05 eV, consistent with the result of Wenthold and Squires. These energetics show that the photodissociation into CH_3^- is energetically possible, however, the observed P(eKE) spectra are definitely not consistent with photodetachment of CH_3^- by a second photon, as very high energy electrons would be produced. In addition, the progressions in the photoelectron spectra[51] recorded by Ellison et al. are not observed in our spectra, further evidence against the photodetachment of CH_3^- by the second photon. If the photodissociation/autodetachment process was occurring, a significant difference between the photoelectron spectra of the stable radical and dissociation products would also be expected, inconsistent with the experimental results. Finally, an autodetachment lifetime of 9−12 ns for vibrationally excited CH_3^- was reported by Mitchell et al.[52] This relatively long lifetime and the internal energy distribution in the CH_3^- photofragments would be

expected to yield a broad eKE distribution in the present fast-beam experimental setup, not the near-threshold P(eKE) spectra obtained at 355 nm. In summary, ionic photodissociation is ruled out as an effectively competing channel in these experiments.

Conclusions

The DPD of $CH_3CO_2^-$ and $CD_3CO_2^-$ has been investigated at 355 and 257 nm. At 355 nm, a near-threshold photoelectron spectrum shows two nearly degenerate states of $CH_3CO_2^\bullet$ (or $CD_3CO_2^\bullet$) with an energy spacing of 0.023 eV and an upper limit to the adiabatic EA $\leq 3.47 \pm 0.01$ eV. Tentative evidence for two other states of $CH_3CO_2^\bullet$, 3.68 and 3.88 eV higher than the ground state of $CH_3CO_2^-$, was also observed at 257 nm. Following photodetachment, both the dissociation channel $CH_3^\bullet/CD_3^\bullet + CO_2$ and stable radicals ($CH_3CO_2^\bullet/CD_3CO_2^\bullet$ or $^\bullet CH_2CO_2H/^\bullet CD_2CO_2D$) were observed, with a branching ratio $\approx$9:1. The similarity of the photoelectron spectra for stable and dissociative products indicates that instead of direct DPD on a repulsive potential energy surface, the nascent $CH_3CO_2^\bullet$ radical undergoes a subsequent yet rapid dissociation. It is proposed that the intermediate state interacts with two or more potential energy surfaces leading to rapid dissociation and the formation of long-lived radicals, respectively. The translational energy release observed in these experiments is large, with $\langle E_T\rangle/E_{avl} = 0.72$ for $CO_2 + CH_3^\bullet$ and $\langle E_T\rangle/E_{avl} = 0.67$ for $CO_2 + CD_3^\bullet$ at 355 nm. High-level ab initio calculations are needed for a more complete understanding of the energetics and dynamics of the prototypical yet complicated acetyloxyl radical.

Acknowledgment. This work was supported by the Department of Energy (DOE) under the Grant No. DE-FG03-98ER14879. Z. Lu thanks M.S. Bowen and X. Zhang for helpful discussions.

References and Notes

(1) Lissi, E. A.; Massiff, G.; Villa, A. E. *J. Chem. Soc., Faraday Trans. 1* **1973**, *69*, 346.
(2) Wang, B.; Hou, H.; Gu, Y. *J. Phys. Chem. A* **1999**, *103*, 8021.
(3) Zhou, Z.; Cheng, X.; Zhou, X.; Fu, H. *Chem. Phys. Lett.* **2002**, *353*, 281.
(4) March, J. *Advanced Organic Chemistry: Reactions, Mechanisms, and Structure*, 4th ed.; John Wiley & Sons: New York, 1992.
(5) Herk, L.; Feld, M.; Szwarc, M. *J. Am. Chem. Soc.* **1961**, *83*, 2998.
(6) Walling, C. *Free Radicals in Solution*; John Wiley & Sons: New York, 1957.
(7) Levy, M.; Szwarc, M. *J. Am. Chem. Soc.* **1954**, *76*, 5981.
(8) Shine, H. J.; Slagle, J. R. *J. Am. Chem. Soc.* **1959**, *81*, 6309.
(9) Herk, L.; Szwarc, M. *J. Am. Chem. Soc.* **1960**, *82*, 3558.
(10) Shine, H. J.; Waters, J. A.; Hoffman, D. M. *J. Am. Chem. Soc.* **1962**, *85*, 3613.
(11) Martin, J. C.; Drew, E. H. *J. Am. Chem. Soc.* **1961**, *83*, 1232.
(12) Martin, J. C.; Taylor, J. W.; Drew, E. H. *J. Am. Chem. Soc.* **1967**, *89*, 129.
(13) Skell, P. S.; May, D. D. *J. Am. Chem. Soc.* **1983**, *105*, 3999.
(14) Braun, W.; Rajbenbach, L.; Eirich, F. R. *J. Phys. Chem.* **1962**, *66*, 1591.
(15) Jaffe, L.; Prosen, E. J.; Szwarc, M. *J. Chem. Phys.* **1957**, *27*, 416.
(16) Holmes, J. L.; Lossing, F. P.; Mayer, P. M. *J. Am. Chem. Soc.* **1991**, *113*, 9723.
(17) Yamdagni, R.; Kebarle, P. *Ber. Bunsen-Ges. Phys. Chem.* **1974**, *78*, 181.
(18) Tsuda, S.; Hamill, W. H. Ionization Efficiency Measurements by the Retarding Potential Difference Method. In *Advances in Mass Spectrometry*; Mead, W. L., Ed.; The Institute of Petroleum: London, 1966; Vol. III, p 249.
(19) Muftakhov, M. V.; Vasil'ev, Y. V.; Mazunov, V. A. *Rapid Commun. Mass Spectrom.* **1999**, *13*, 1104.
(20) Wentworth, W. E.; Chen, E.; Steelhammer, J. C. *J. Phys. Chem.* **1968**, *72*, 2671.
(21) Ding, C.-F.; Wang, X.-B.; Wang, L.-S. *J. Phys. Chem. A* **1998**, *102*, 8633.
(22) Kikuchi, O.; Utsumi, K.; Suzuki, K. *Bull. Chem. Soc. Jpn.* **1977**, *50*, 1339.
(23) Peyerimhoff, S. D.; Skell, P. S.; May, D. D.; Buenker, R. J. *J. Am. Chem. Soc.* **1982**, *104*, 4515.
(24) Sicilia, E.; Maio, F. P. D.; Russo, N. *J. Phys. Chem.* **1993**, *97*, 528.
(25) Rauk, A.; Yu, D.; Armstrong, D. A. *J. Am. Chem. Soc.* **1994**, *116*, 8222.
(26) Yu, D.; Rauk, A.; Armstrong, D. A. *J. Chem. Soc., Perkin Trans. 2* **1994**, 2207.
(27) Kieninger, M.; Ventura, O. N.; Suhai, S. *Int. J. Quantum Chem.* **1998**, *70*, 253.
(28) Kim, E. H.; Bradforth, S. E.; Arnold, D. W.; Metz, R. B.; Neumark, D. M. *J. Chem. Phys.* **1995**, *103*, 7801.
(29) Clements, T. G.; Continetti, R. E. *J. Chem. Phys.* **2001**, *115*, 5345.
(30) Continetti, R. E. *Int. Rev. Phys. Chem.* **1998**, *17*, 227.
(31) Deyerl, H.-J.; Alconcel, L. S.; Continetti, R. E. *J. Phys. Chem. A* **2001**, *105*, 552.
(32) Alconcel, L. S.; Deyerl, H.-J.; DeClue, M.; Continetti, R. E. *J. Am. Chem. Soc.* **2001**, *123*, 3125.
(33) Davies, J. A.; LeClaire, J. E.; Continetti, R. E.; Hayden, C. C. *J. Chem. Phys.* **1999**, *111*, 1.
(34) Bowen, M. S.; Continetti, R. E. *J. Phys. Chem. A*, in press.
(35) Sherwood, C. R.; Continetti, R. E. *Chem. Phys. Lett.* **1996**, *258*, 171.
(36) Ashfold, M. N. R.; Lambert, I. R.; Mordaunt, D. H.; Morley, G. P.; Western, C. M. *J. Phys. Chem.* **1992**, *96*, 2938.
(37) Gendron, D. J.; Hepburn, J. W. *J. Chem. Phys.* **1998**, *109*, 7205.
(38) Zare, R. N. *Mol. Photochem.* **1972**, *4*, 1.
(39) Hanold, K. A.; Garner, M. C.; Continetti, R. E. *Phys. Rev. Lett.* **1996**, *77*, 3335.
(40) Wenthold, P. G.; Squires, R. R. *J. Am. Chem. Soc.* **1994**, *116*, 11890.
(41) *Tables of molecular vibrational frequencies*; Shimanouchi, T., Ed.; National Bureau of Standards: Washington, DC, 1972.
(42) *NIST Chemistry WebBook, NIST Standard Reference Database Number 69* (http://webbook.nist.gov/chemistry/); Mallard, W. G., Ed.; National Institute of Standards and Technology: Gaithersberg, MD, 2003.
(43) Symons, M. C. R. *J. Am. Chem. Soc.* **1983**, *87*, 1833.
(44) Wormhoudt, J.; McCurdy, K. E. *Chem. Phys. Lett.* **1989**, *156*, 47.
(45) Sears, T. J.; Frye, J. M.; Spirko, V.; Kraemer, W. P. *J. Chem. Phys.* **1989**, *90*, 2125.
(46) Herzberg, G. *Molecular Spectra and Molecular Structure Vol. II Infrared and Raman Spectra of Polyatomic Molecules*; Krieger Publishing: Malabar, FL, 1991.
(47) Busch, G. E.; Wilson, K. R. *J. Chem. Phys.* **1972**, *56*, 3626.
(48) Trentelman, K. A.; Kable, S. H.; Moss, D. B.; Houston, P. L. *J. Chem. Phys.* **1989**, *91*, 7498.
(49) Compton, R. N.; Reinhardt, P. W.; Cooper, C. D. *J. Chem. Phys.* **1975**, *63*, 3821.
(50) Knapp, M.; Echt, O.; Kreisle, D.; Mark, T. D.; Recknagel, E. *Chem. Phys. Lett.* **1986**, *126*, 225.
(51) Ellison, G. B.; Engelking, P. C.; Lineberger, W. C. *J. Am. Chem. Soc.* **1978**, *100*, 2556.
(52) Mitchell, S. E.; Conklin, P. M.; Farley, J. W. *J. Chem. Phys.* **2003**, *118*, 11017.
(53) Grabowski, J. J.; Cheng, X. *J. Am. Chem. Soc.* **1989**, *111*, 3106.